Supplementary Material

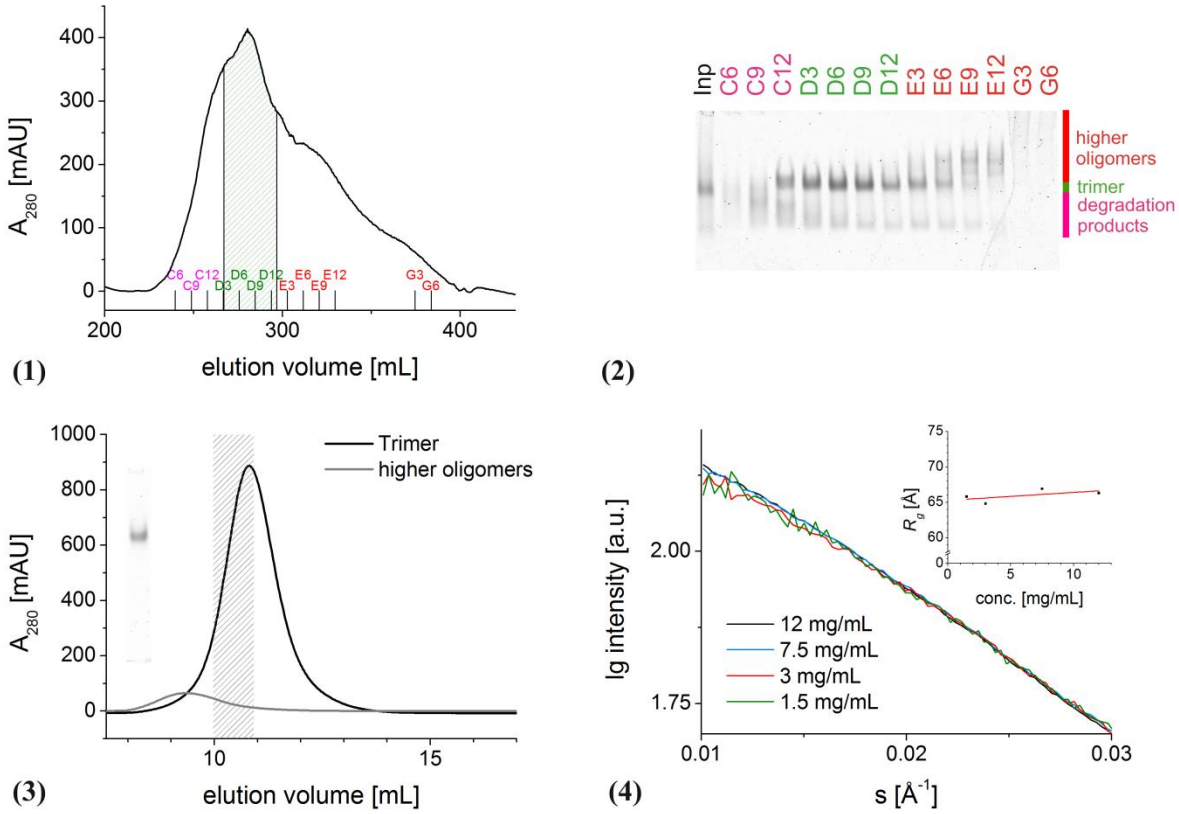

Supplementary Figure S1. Gephyrin sample quality. (1) Chromatogram resulting from anion exchange chromatography of full-length gephyrin. Only the green shaded fractions were used for the subsequent size exclusion chromatography step. A_{280} is the abbreviation for the absorbance at 280 nm. (2) The gel corresponding to the chromatogram displayed in (1). In separate experiments we observed that gephyrin species above the dominant trimeric fraction are presumably higher oligomers (data not shown). Bands below the trimers correspond to degradation products. Conservative pooling led to a depletion of higher oligomers, as can be deduced from (3) which displays a typical chromatogram of the final size exclusion chromatography step immediately before the SAXS and AFM experiments, for which only fractions were pooled that are marked by the grey shaded area. This representation also shows that conservative pooling almost eliminated residual higher oligomers. The native PAGE gel confirms sample homogeneity. (4) The superposition of the curves recorded at different concentrations and the R_g vs. concentration plot in the inset argue for a slight concentration dependence but against the formation of higher gephyrin oligomers within the given range of 1.5 mg/mL to 12 mg/mL.

Supplementary Table S1. Results of the composition profiler analysis of gephyrin's linker region. Gephyrin's linker region was tested for depletion or enrichment of different amino acid groups. The reference was composed of the folded terminal domains, GephG and GephE. The arrows indicate whether a certain amino acid group is enriched (⇧) or underrepresented (⇩) in the linker region in comparison to the rest of the protein. *n. s*. stands for *not significant*.

aromatic content	⇩	P-value=0.036131 (≤0.050000)
charged residues	*n. s.*	P-value=0.489564 (>0.050000)
positively charged	*n. s.*	P-value=0.361978 (>0.050000)
negatively charged	*n. s.*	P-value=0.957056 (>0.050000)
polar (Zimmerman)	*n. s.*	P-value=0.426580 (>0.050000)
hydrophobic (Eisenberg)	⇩	P-value=0.000206 (≤0.050000)
hydrophobic (K-D)	⇩	P-value=0.004108 (≤0.050000)
hydrophobic (F-P)	*n. s.*	P-value=0.105977 (>0.050000)
exposed (Janin)	⇧	P-value=0.000012 (≤0.050000)
flexible (Vihinen)	⇧	P-value=0.015851 (≤0.050000)
high interface prop. (J-T)	⇩	P-value=0.000087 (≤0.050000)
high solvation poten. (J-T)	⇧	P-value=0.000137 (≤0.050000)
frequent in α-helices (N)	*n. s.*	P-value=0.443595 (>0.050000)
frequent in β-strands (N)	⇩	P-value=0.001125 (≤0.050000)
frequent in coils (N)	⇧	P-value=0.021165 (≤0.050000)
high linker propensity (G-H)	*n. s.*	P-value=0.883961 (>0.050000)
disorder promoting (Dunker)	⇧	P-value=0.000029 (≤0.050000)
order promoting (Dunker)	⇩	P-value=0.000167 (≤0.050000)
bulky (Zimmerman)	⇩	P-value=0.003376 (≤0.050000)
large (Dawson)	⇩	P-value=0.022792 (≤0.050000)

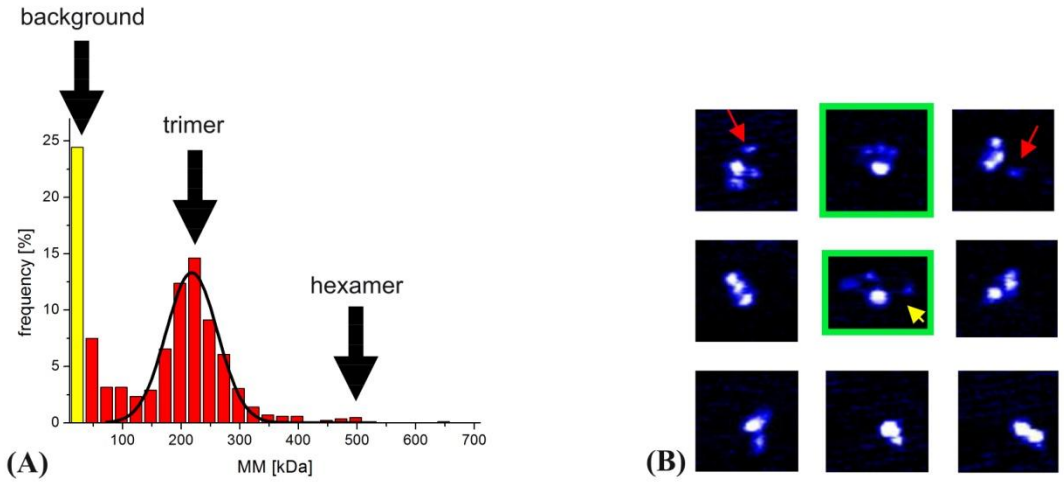

Supplementary Figure S2. Supporting AFM analysis. (A) The relative frequencies of all AFM depositions were averaged. In the images a significant fraction of the particles possesses apparent molecular masses of < 40 kDa (indicated by the yellow bar). A high sample purity (Appendix A), several AFM control experiments on full-length gephyrin as well as the individual domains (data not shown) and the fact that the contribution of this apparent species varied from deposition to deposition (between 3% and 29%) led us to interpret this small apparent species as neither a degradation product nor a contamination but instead it is due to different (experimentally induced) background levels. (B) Typical examples for 1-, 2-, 3- and 4-segmented particles observed in AFM micrographs. Red arrows mark small particles, which were considered to be part of the adjacent particles, if they were in close spatial proximity. This approach is justified by the longest linkers that could be resolved (marked by the yellow arrow). The image excerpts highlighted with a green frame exemplify that the different appearance of the gephyrin particles are not simply a projection artefact, as these two particles are not congruent – no matter which rotations and/or translations would be performed.

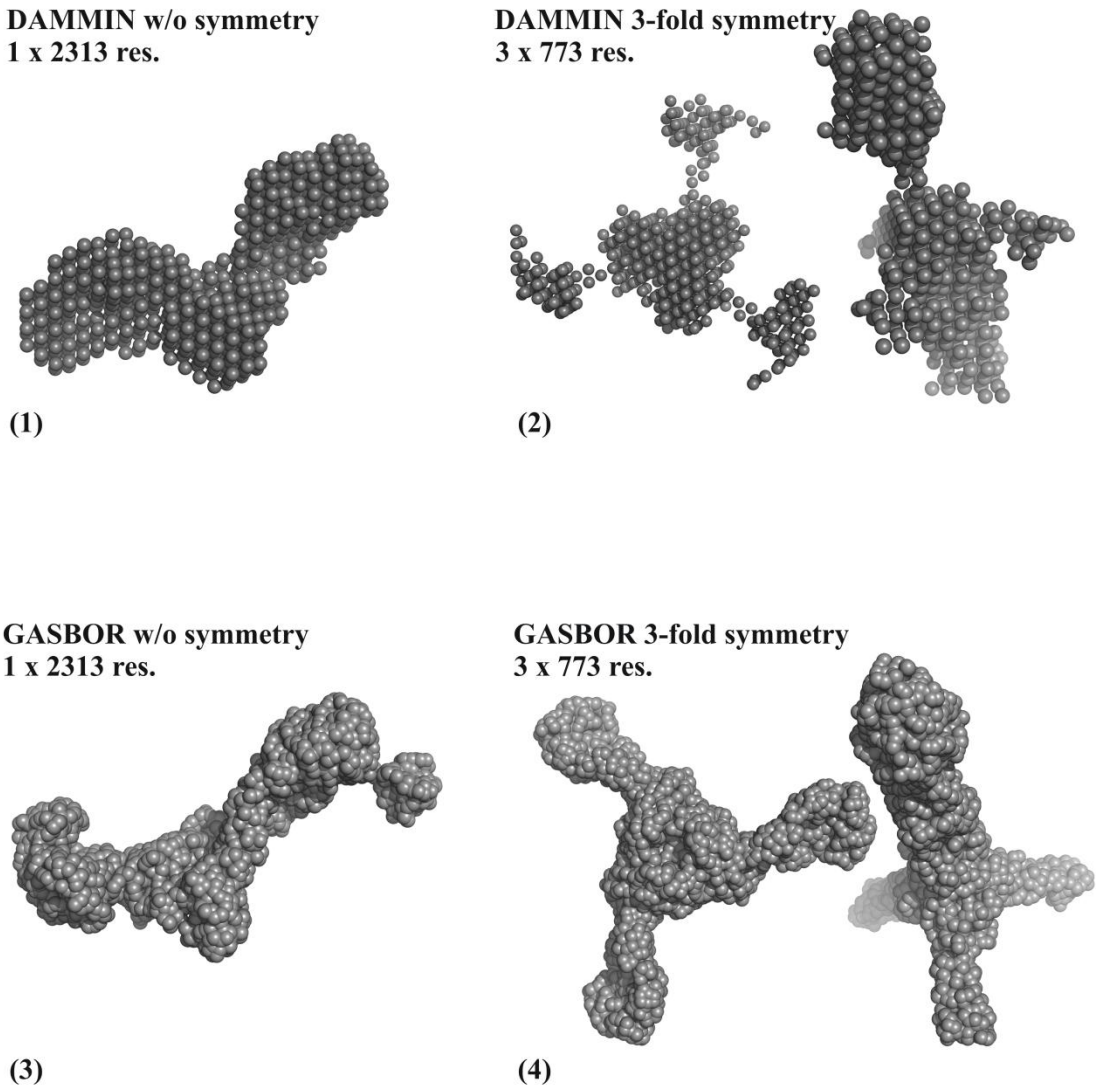

Supplementary Figure S3. SAXS *ab initio* modelling. *Ab initio* models obtained with DAMMIN (A & B) and GASBOR (C & D). Elongated models were obtained with unconstrained modelling (A & C). The inclusion of a threefold symmetry constraint led to three-pronged star-like assemblies (B & D), it should be noted, that rod-like structures as shown in B were obtained to almost the same extent in DAMMIN (five of ten models) and DAMMIF calculations (six of ten models, not shown), but not with GASBOR.

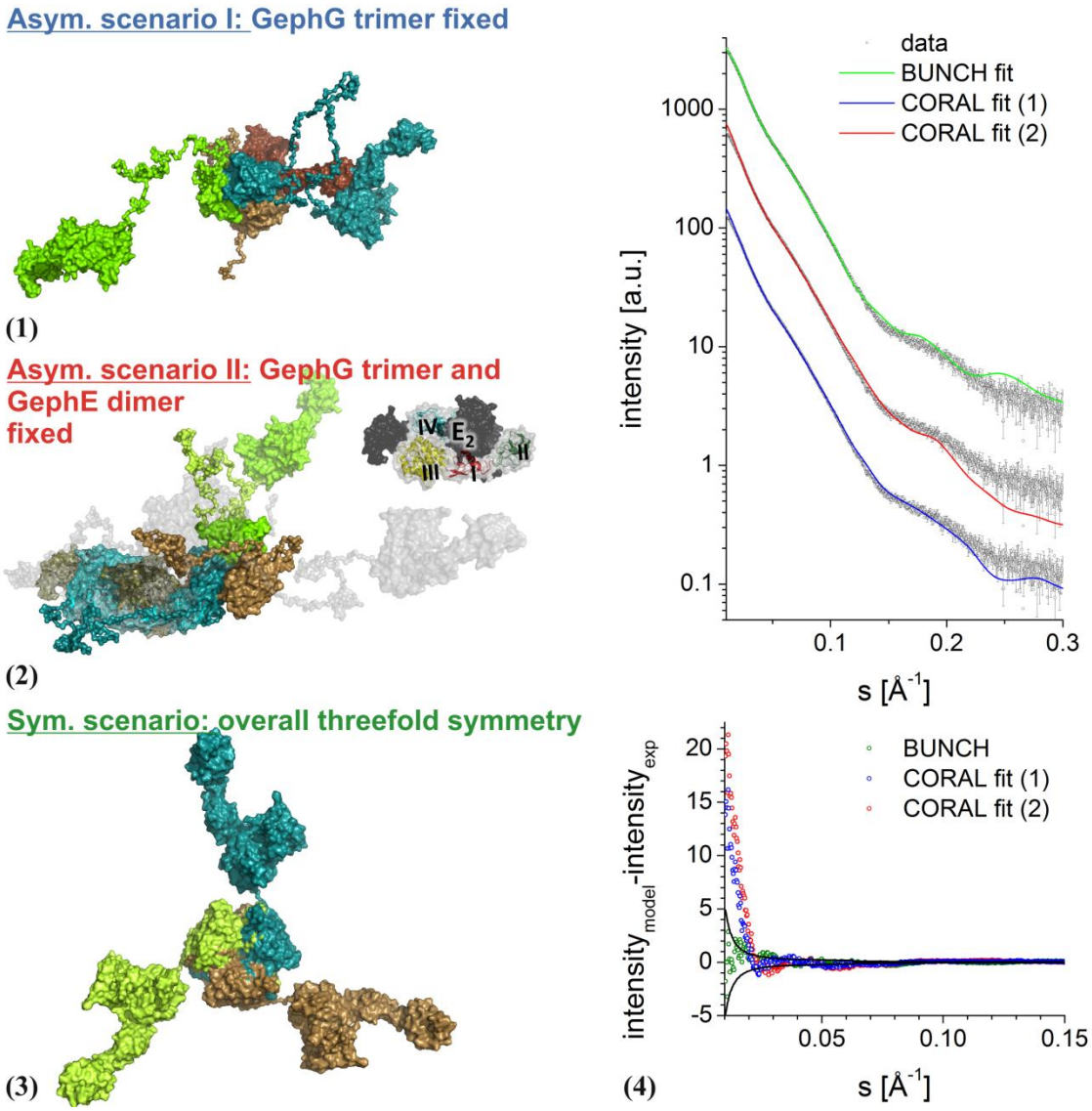

Supplementary Figure S4. Rigid body modelling. Unconstrained rigid body modelling in terms of overall symmetry was conducted with CORAL. In **asymmetric scenario I**, no symmetry was assumed outside the GephG trimer ($GephG_3$). In the resulting model domains are arranged like beads on a string (1). The dark brown GephE is not represented in exactly the same color as GephG and the linker but slightly darker to allow the distinction between these parts. In a next step (**asymmetric scenario II**), we assumed not only that the GephG trimer interface is fixed but also one GephE dimer interface is maintained (E_2 in (2)), leaving one isolated GephE monomer. As expected, these rigid body models are also elongated, however, they differ from asymmetric scenario I in that the overall dimensions are smaller. Two alternative models are superposed using the GephE dimer as a template (one in yellow and one in salmon), exemplifying that the models did not converge towards a single solution (2). For the **symmetric scenario** BUNCH was used and the model dimensions correlate well with the GNOM-derived R_g and D_{max} values (3). While for CORAL modelling the R_g had to be imposed, this was not required in the case of BUNCH. Although the fit for the symmetric scenario was superior over the asymmetric scenarios (4), the obtained rigid triskelion is – especially in light of

the AFM data – not a suitable model to describe a flexible assembly like gephyrin which is also indicated by a rather high values for the average χ (1.5) and the NSD (1.52 ± 0.17). Pink arrows indicate the maximum interatomic distance D_{max}.

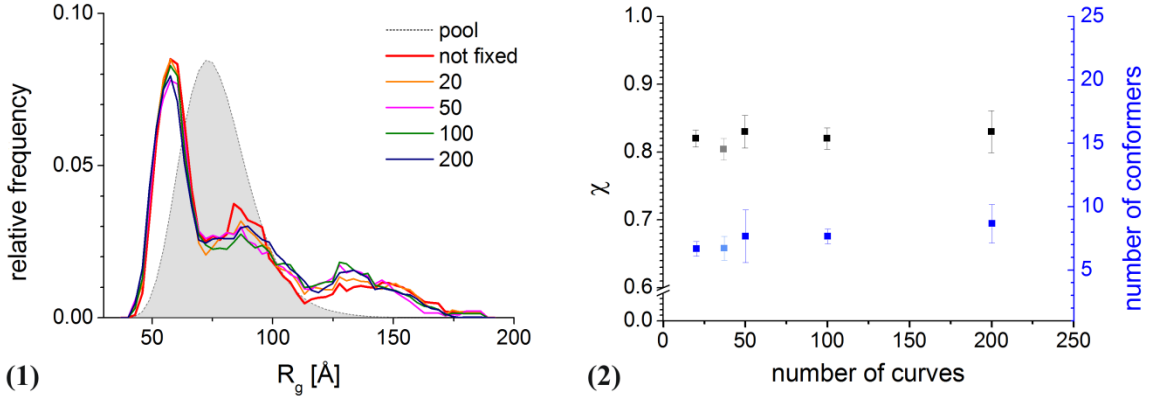

Supplementary Figure S5. Supporting SAXS EOM analysis. In a previous study it has been reported, that the EOM R_g distribution can vary with the number of conformers (Boze *et al.*, 2010). This study was performed with EOM 1.3. This behaviour is well known, and this is one of the reasons that made us use an enhanced version - EOM 2.0 (Petoukhov *et al.*, 2012, Tria *et al.*, 2012). In this later version, the optimum number of curves that belong to the ensemble is automatically detected, and it is the result of millions of ensembles with randomly distributed size. In the present work, the final number of conformers selected by EOM 2.0 is six (each one with its own weight), and this represents likely the best combination of models in order to recreate the volume occupied by the protein in solution. To test whether the R_g distribution depends on the number of curves per ensemble (abbreviation: N), the latter was varied. The results revealed that the final R_g distributions tended to remain unaffected by the number of curves (F1), providing proof of principle. Here, "not fixed" refers to the ensemble described in the main text of the manuscript with a χ of 0.8 (section 3.3.3). The χ values were likewise unaffected by the number of fixed curves as indicated by the corresponding χ vs. N plot (F2). At the same time we added the number of conformers derived from the different runs which is ~7 on average with hardly any variation regarding the number of curves. EOM calculations were performed in triplicates for the merged data which allowed us to include error bars.